Seismic monitoring of crush pillar behaviour in a deep-level gold mine using active sources

Yolanda Chambati [a,*], Mark Green [b], Bryan Watson [c], Peter G Andrews [d]

[a] *South Deep Gold Mine, Gold Fields, South Africa*

[b] *Institute of Mine Seismology, South Africa*

[c] *University of the Witwatersrand, South Africa*

[d] *Corporate Technical Services, Gold Fields, Australia*

Abstract

Gold Fields, South Deep Gold Mine uses crush pillars in their deep-level operation to support de-stress stopes. There was a concern about the ability of these pillars to withstand dynamic closure due to seismic events that are common at that depth. A study was conducted at approximately 3,000 m below the surface to determine the dynamic behaviour of these pillars. This paper describes active seismic source monitoring that was used to determine changes that developed within the pillar during a seismic event. The results showed that the crush pillar responded dynamically to large events, even when fully formed. These seismic events induced large decreases in seismic velocity measured using active sources. These drops were followed by a characteristic post-seismic relaxation, indicative of material damage followed by gradual healing. No evidence of permanent 'damage' was observed; however, no very large (moment magnitude greater than 2) seismic events occurred during the monitoring period.

Keywords: crush pillar, seismic, deep mine, de-stress, rockbursts

1 Introduction

South Deep is a mechanised mine, extracting a wide reef at a depth of approximately 3,000 m below the surface. Such wide reefs have not been mined at this depth elsewhere in the world and the production layouts developed at the mine are therefore unique. South Deep is situated approximately 45 km west of Johannesburg in the West Witwatersrand mining region (Figure 1). The mining area covers 4,232 hectares and extends for 9.5 km north–south and 4.5 km east–west at its widest points.

**Figure 1   Location of South Deep mine**

---

* Corresponding author.

A series of layered overlapping horizontal de-stress cuts are used to de-stress the large orebody target horizons as shown in Figure 2. Access to the de-stress cut is obtained through a spiral decline, which is sited beneath a previously mined de-stressed area. De-stress cuts consist of 6 m wide × 5.5 m high bords and 7 m wide × 20 m long crush pillars. Mining must be optimally sequenced to mitigate rockburst and stress damage. This de-stress cut is subsequently integrated with sequential longhole stoping by utilising the de-stress cut drives as longhole drives (Figure 2). This layout allows for selective mining in the massives where there may be sub-economic quartzite middlings.
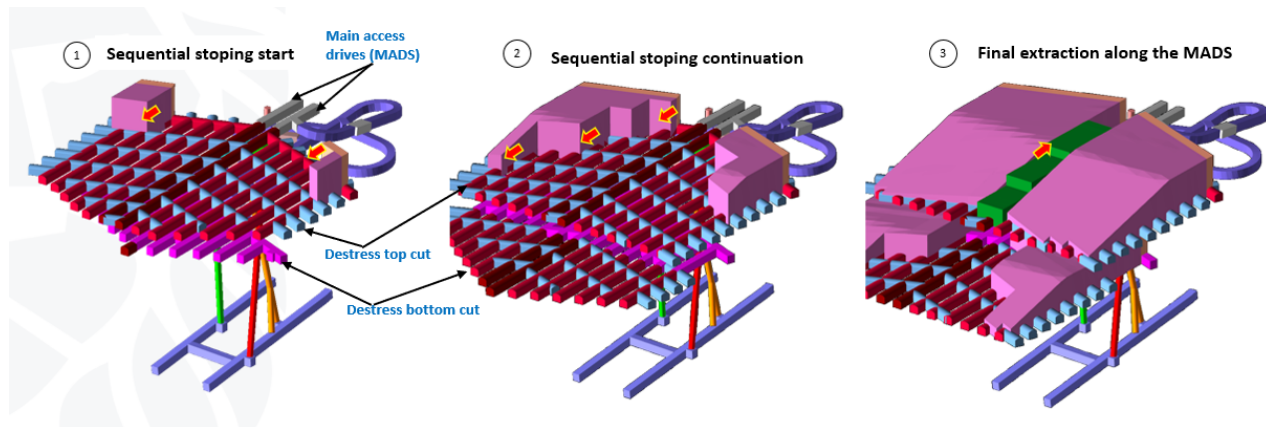
Figure 2   Isometric view of the horizontal de-stress and stoping layout

Crush pillars were introduced to the de-stress stopes of South Deep Gold Mine (SD) to improve efficiencies in the destressing stopes (Watson et al. 2014). The behaviour of crush pillars has been studied in the platinum mines (Watson et al. 2010), and the findings were adapted to the different environment at SD. One of the most significant differences was the comparatively large closure rate at SD, with occasional rapid seismic loading typical of a deep mining environment. The quartzite rocks of the Witwatersrand gold mines are more brittle than the platinum mines, suggesting that the tolerance on design parameters may also be comparatively smaller (because a stiffer loading environment is required for stable failure, which is achieved close to the advancing face). One of the concerns of the mine was how the crush pillars would behave when loaded dynamically during a seismic event. This paper describes an active seismic source monitoring project designed to monitor the behaviour of the crush pillars during and after a seismic event.

2   Monitoring method

Active seismic sources were used to monitor a selected pillar. Active seismic source tomography is a technique used to image subsurface structures and properties by analysing the propagation of seismic waves generated by controlled sources. This technique is also known as a method to create a 2D velocity map (Figure 3). It involves the deployment of seismic sources at various locations to generate seismic waves that propagate through the seismic medium. These waves are recorded by a network of receivers, and tomographic algorithms are then applied to reconstruct the velocity model based on the recorded data (Green 2023). This model will indicate the fracture state of different parts of the pillar and how it changes over time.

Application of active seismic sources for pillar monitoring in deep mines has been trialled at Mponeng gold mine in South Africa and at El Teniente copper mine in Chile (Lynch 2010, 2012). The field trials at these sites demonstrated that active seismic sources provided a reliable means of inducing controlled seismic waves within the rock mass. The recorded data allowed for accurate detection, localisation and analysis of changes in the rock, leading to a better understanding of the rock mass in response to mining at these mines. Active seismic sources in microseismic monitoring offer several advantages over passive monitoring methods. Active sources allow for controlled and repeatable experiments, enabling a study of changes in rock fracture density over time (Chelminski et al. 2019). This approach facilitates a deeper understanding of pillar response to dynamic loading conditions.
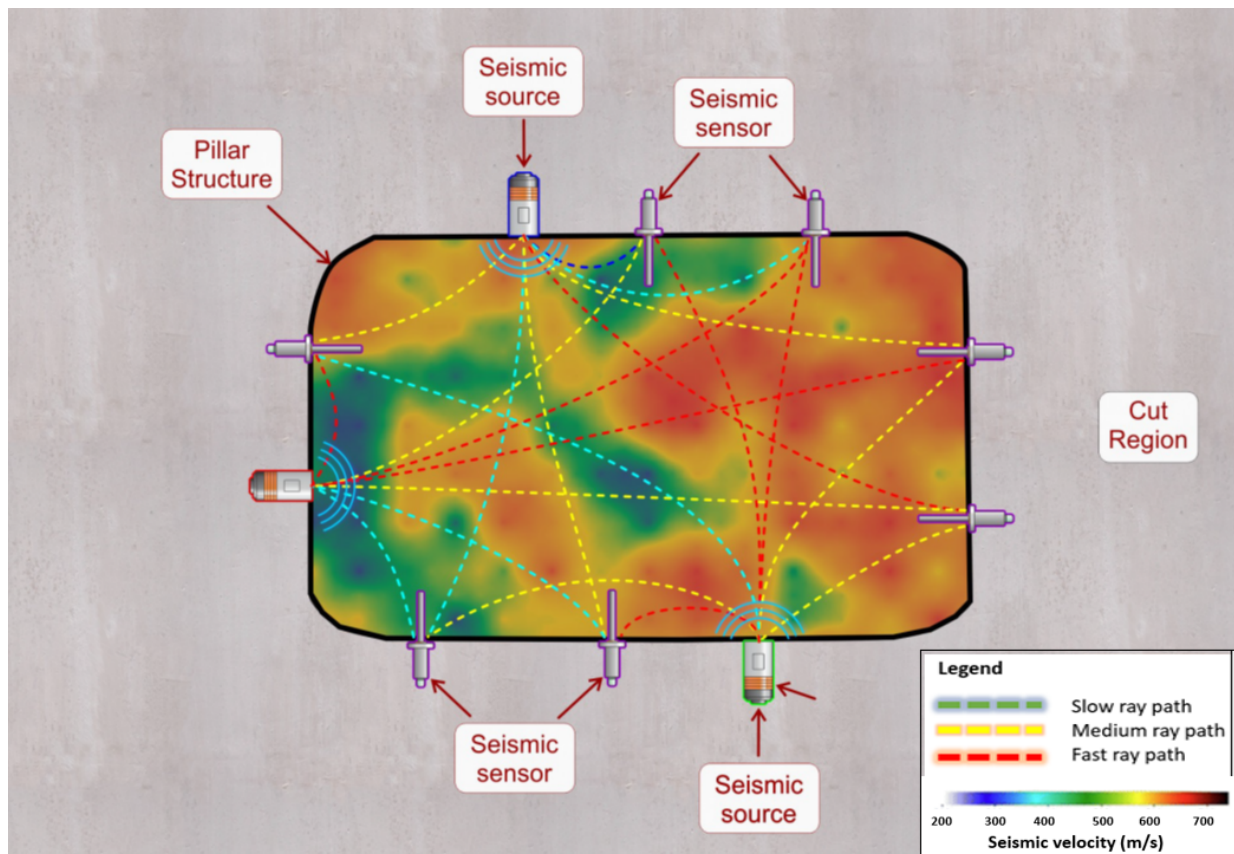
Figure 3   Schematic 2D velocity map for an active source pillar under monitoring

For this study, the controlled seismic signals were generated by surface-mounted pneumatic and piezoelectric sources. The resulting source signals were recorded and analysed to determine changes within the pillar, the mechanism is illustrated in Figure 4. A surface-mounted impacting pneumatic source includes a stand-alone air supply that provides locally compressed air to the pneumatic source equipment. The stand-alone supply is more versatile in location and produces more consistent outputs than the compressed air mainlines of a mine. The output energy of impacting pneumatic sources is lower when compared to other existing seismic sources (airguns, explosives, etc, Chelminski et al. 2019), however, this is not an issue for smaller-scale surveys. The high repeatability of the source signals means that these sources can also benefit from signal stacking techniques to improve signal-to-noise ratios (SNR).
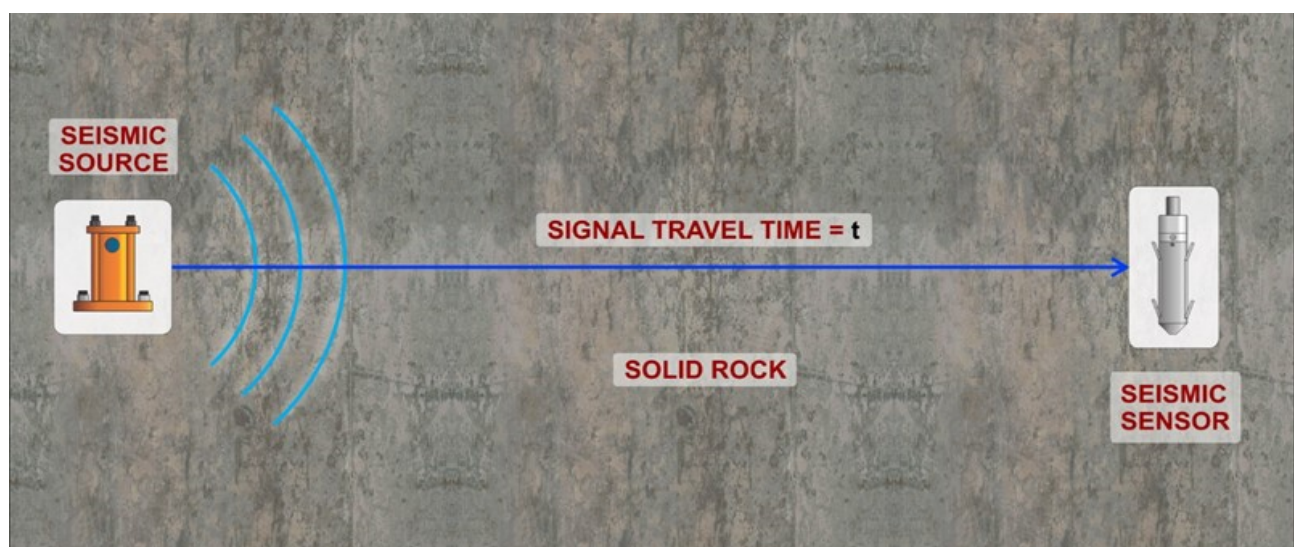
Figure 4   Illustration of active source pillar monitoring

A piezoelectric source is a seismic source type that operates using the piezoelectric effect whereby a piezoelectric material undergoes a change in volume, in response to an applied voltage. This effect can be used to generate a vibration in rock with very precise control over the signal generated. The piezoelectric source is weaker than the pneumatic source and operates at higher frequencies, which makes it better suited to studying media of smaller dimensions (Silver et al. 2007). It also generates a highly repeatable and stable signal which makes it ideal for data stacking and long-term monitoring. The piezoelectric source is operated by a piezoelectric source driver which generates a high voltage of ±900 Volts direct current pulse (Lynch 2010).

Post-seismic relaxation, also known as after-slip or viscoelastic relaxation, refers to the gradual deformation or adjustment of the rock mass following a major earthquake. It is a process that occurs after the initial seismic event and can continue for weeks, months, or even years. The process starts with rock mass damage from the seismic event and is typically followed by a healing process whereby fractures gradually start closing again. Post-seismic relaxation is a result of the redistribution of stress and the response of the rock mass to the released strain energy during the seismic event (Green 2023). This phenomenon was observed on the San Andreas Fault after earthquakes with magnitudes 6.5 and 6.0, respectively (Brenguier et al. 2008).

3   Instrumentation site

3.1   Project set up

A partially formed pillar was instrumented with a surface-mounted pneumatic impacting source and a series of surface-mounted uniaxial 14 Hz geophones, positioned around the exposed section of the pillar (Figure 5 and Figure 6). The typical footprint of these pillars is approximately 7 m wide and 20 m long, making source-to-sensor distances relatively short. The expected crush state of the subject pillar (heavily fractured) necessitated the design of specialised 1.1 m long mounting anchors for the sensors. These anchors were installed in 20 mm diameter boreholes. As the cutting of the pillar proceeded, additional sensors were added to the pillar surface. A sensor was also installed adjacent to each source, which served as a reference that allowed for signal zero-time measurement.
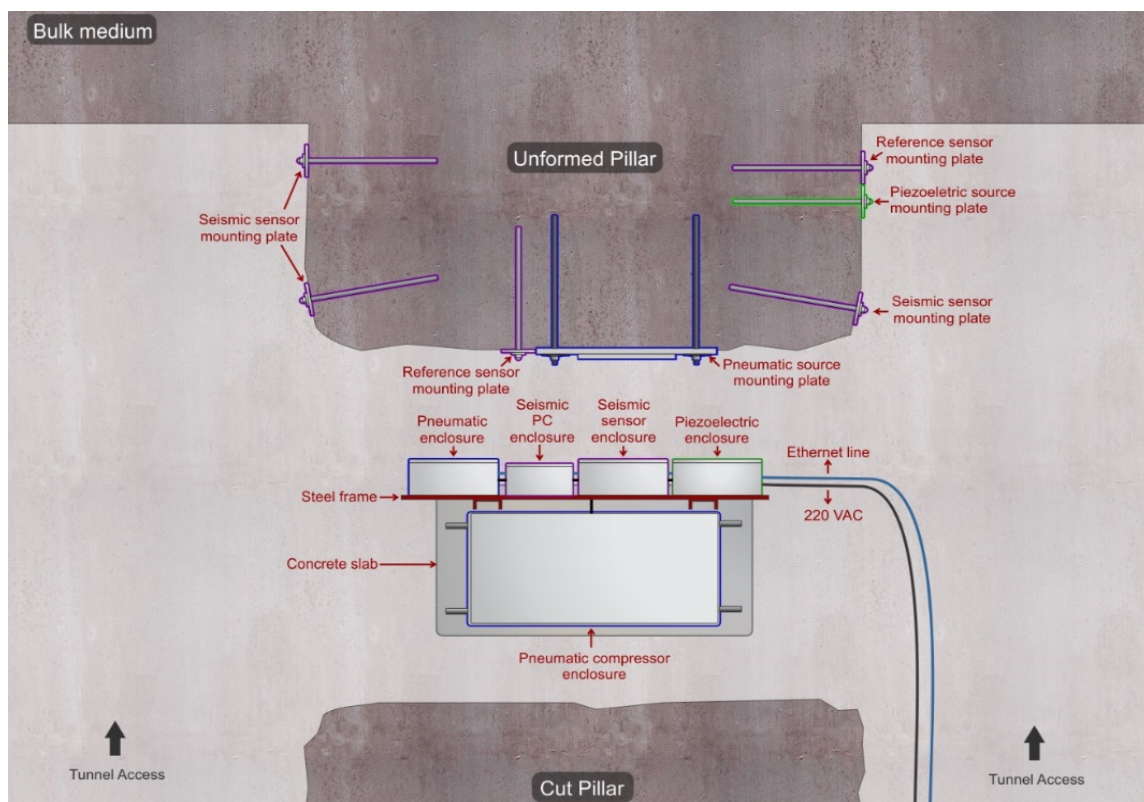
Figure 5   An illustration of the planned design layout of the project hardware for a partially formed pillar

Figure 6 Plan view of the crush pillar project site, showing the surveyed locations of the mounting anchors for both sources and sensors

The relatively small size of the pillar provided a good opportunity to incorporate a piezoelectric source and compare its performance to the pneumatic impacting source. The piezoelectric source was a hydroacoustic projector that normally operates in a water-filled borehole. To accommodate this source, a bespoke water-filled boat was designed and mounted on the sensor anchors. Technical difficulties were expected due to the difficulty of instrumenting an uncut pillar in an active working place. Site preparation, which included enclosure mounting, anchor installation and provision of power and Ether communications, was completed in October 2022. Installation of active sources, sensors, data acquisition and source driver hardware were completed in early November 2022 (Figure 7).

Figure 7 Underground photo of the pillar monitoring site and hardware enclosures

3.2   Data recording

Recording of continuous data sampled at 24 kHz, started in early November 2022. Both the pneumatic and piezoelectric sources were brought online with the pneumatic source set to fire once every two minutes and the piezoelectric set to fire three times a second. All continuous data was routinely transferred to the Institute of Mine Seismology (IMS) database servers where it underwent signal processing and travel time variation analysis.

Data recording was severely affected by several issues, the most persistent being problems related to mains power and data communications at the project site. The project also suffered physical damage to monitoring hardware and cabling due to the proximity of active mining and tramming. The piezoelectric source signal cable was damaged soon after 15 December 2022. After the cable was repaired, the signal performance was greatly reduced making signal recovery difficult. Reduced signal recovery was probably due to damage to the source mounting or the source itself.

4   Processing

4.1   Active source tomography

Signal processing included various techniques, which were aimed at enhancing, analysing, and extracting information from the signals they produce. The propagation of seismic waves at the project site were localised and analysed using the signal travel time analysis. It was suggested by Green (2023) and Silver et al. (2007) that if the seismic medium undergoes change, it will influence the signal travel time. Measuring the change in signal travel time allows us to infer how the medium changed.

4.2   Signal extraction

The first step in data processing was the extraction of the source signal from the continuous records. The occurrence time of signals was identified in the continuous seismogram record using data from the two reference sensors installed next to the sources (Site 404 and 406 in Figure 8), which recorded the source signal close to its time of initiation. The identification process employed a combination of the amplitude threshold peak detection, followed by a sliding window Pearson's cross-correlation of a candidate shot against a predefined reference waveform (Niu et al. 2008). The cross-correlation provided both a measure of waveform similarity and the precise point of time alignment between the candidate and reference shots.
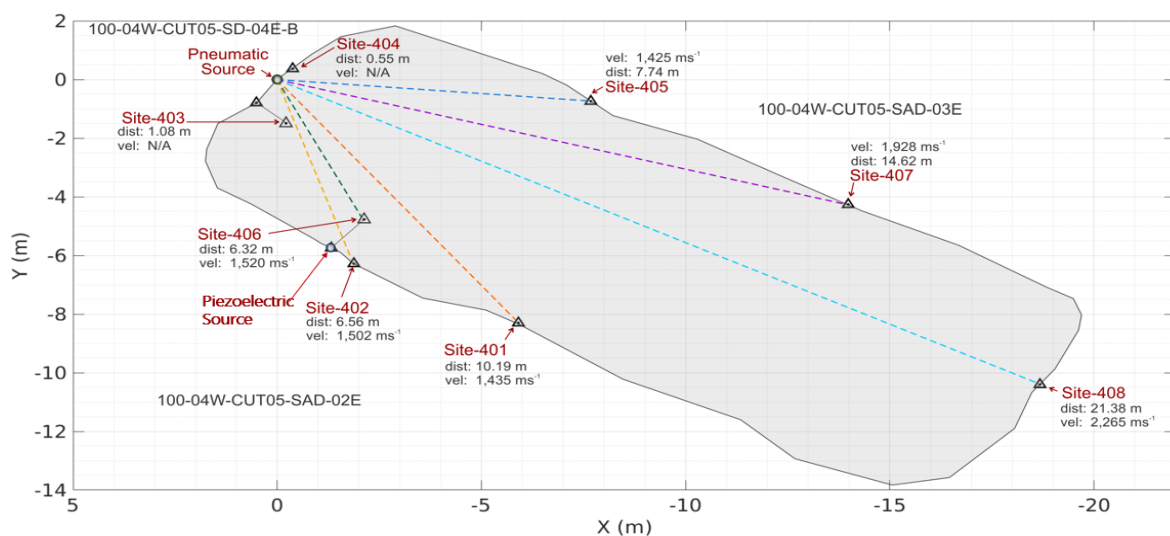
Figure 8   Plot of final source and sensor locations and ray paths for the pneumatic source (note that pillar shape is approximated based on sensor locations)

Cross-correlation functions in statistics give a measure of association between signals. The cross-correlation coefficient, also known as Pearson's correlation coefficient, measures the linear relationship between two variables. It ranges from −1 to 1 (Niu et al. 2008):

where:

r = 1: perfect positive linear correlation

r = −1: perfect negative linear correlation

r = 0: no linear correlation (i.e. variables are independent).

A sliding window approach was incorporated with the cross-correlation to help ensure optimal alignment between the two signals. If a candidate shot had a high Pearson value (> 0.8) then it was marked as valid, and the shot time was used to extract a data slice with a fixed length that contained data from all sensors in the experiment.

4.3 Data stacking

Accurate signal travel time change measurement was dependent on signal quality, namely the signal amplitude compared to recorded noise. The SNR can be improved using data stacking, which is the process of adding two or more similar and phase-aligned signals together, resulting in a stack. The signal portion of the stack will grow as a factor of the number of signals stacked together. Noise on the other hand is uncorrelated and will tend to grow on average by a factor of the square root of the number of the signals stacked. Stacking thus causes SNR to grow by a factor $\sqrt{n}$ where n is the number of signals stacked. Stacking is particularly important for the piezoelectric source, which outputs a high-frequency signal at low power, giving it a very limited range. However, the source generates identical signals, at a rapid rate making it ideal for data stacking. To help reduce data volumes during velocity variation analysis, stacking was applied to both data recorded from the pneumatic and piezoelectric sources.

4.4 Phase delay methods

Changes in seismic velocity are inversely proportional to changes in signal travel time as given by the linear travel equation:

$$V = d/\text{T} \tag{1}$$

Where:

V = velocity (m/s)

d = distance (m)

T = time (s)

The travel time variation was measured by calculating the phase lag difference between stacked signals that were comprised of data recorded at different points in time. For this analysis, the sliding window cross-correlation method was used to measure the signal delay or phase lag between two similar, yet time-shifted signals (Niu et.al 2008; Mikesell et al. 2015; Silver et al. 2007). The Pearson Cross-Correlation Function (CCF) of two waveforms for the specified time window between t0 and t1 is given by (Equation 2):

$$\text{CCF}(t, r) = \frac{\sum_{t0}^{t1} [f(t)\, g(t + \tau)]}{\sqrt{\sum_{t0}^{t1} [f(t)]^2 \sum_{t0}^{t1} [g(t + \tau)]^2}} \tag{2}$$

In Equation 2, let f(t) be the time series of the reference waveform and g(t) be the subject waveform, which is time delayed such that for any ti there is an associated phase lag, i.e. f (ti) = g (ti + τ) is evaluated for a range of values for τ, the sliding window offset resulting in what is commonly referred to as the CCF. The point of maximum in the CCF will coincide with the applied phase lag for which two time-shifted signals are phase-aligned (Figure 9). Cubic spline interpolation was used to oversample stacked waveforms to measure

phase lag changes smaller than the inter-sample time afforded by the hardware sampling rate of 24 kHz (Bartels et al. 1987).


(a)   (b)
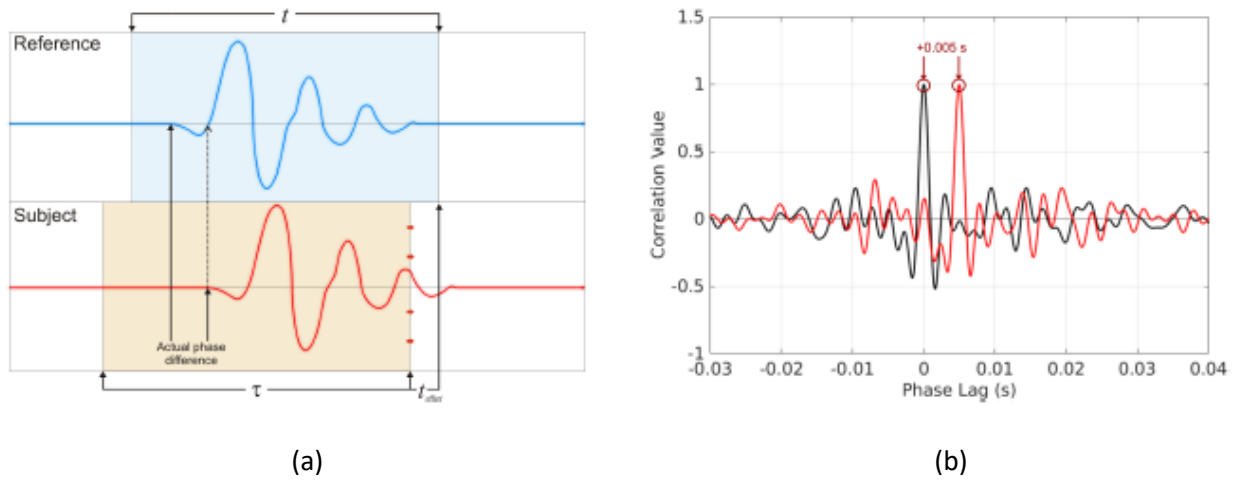
Figure 9   A sliding window for the candidate signal (a) showing a measure of similarity between the waveforms for different applied phase lags, resulting in the cross-correlation function (b)

5   Results and discussion of results

5.1   Absolute seismic velocity

Absolute seismic velocity was calculated by measuring the source signal's first phase arrival at all pillar sensors, using both the pneumatic and piezoelectric sources (Figure 10). The difference between the arrival times of the respective source's reference sensor and other sensors, yielded the signal time of flight from which velocity was calculated. It should be noted that both the sources and the various sensors were operational at different points in time, so not all velocity measurements were made at the same point in time. Comparison of absolute velocity measurements between 5 November 2022 and 5 April 2023, showed an overall increase in seismic velocity (5 to 30%), which implied that the pillar underwent healing or stiffening during that period.
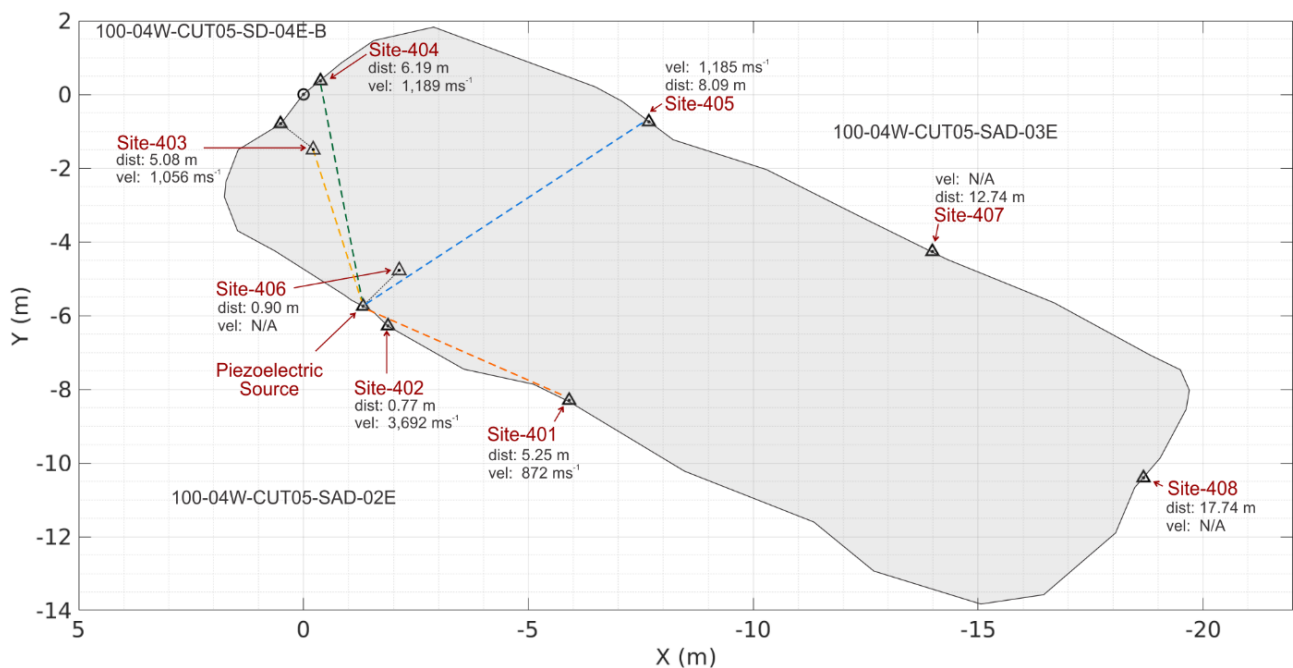

Figure 10   Seismic velocities (average) measured using the piezoelectric source signal

5.2 Seismic velocity variation

Sliding window cross-correlation was applied to stacked signals using Equation 2, and seismic velocity change analysis was performed on data from both the piezoelectric and pneumatic sources. Processing of the data also revealed that the source signal waveform changed over time (greater than seven days). To help counter this, an adaptive reference scheme was adopted, which gradually updates the reference waveform. This adaptive reference method has the drawback of suppressing velocity changes that would have occurred over a long-term. The two sources were never fully operational at the same time; therefore, no direct comparison of the two devices was possible.

5.2.1 Piezoelectric source

Viable piezoelectric seismic source data, captured between the 5–18 November 2022 and, was used for seismic velocity variation analysis. Large gaps in the data are present during this period, due to temporary power or communications loss, or periods of excessive noise. The calculated velocity variation log is presented graphically in Figure 11. Data recording from the piezoelectric source continued after the 18 November, however, reliable signal recovery from this data was not possible.
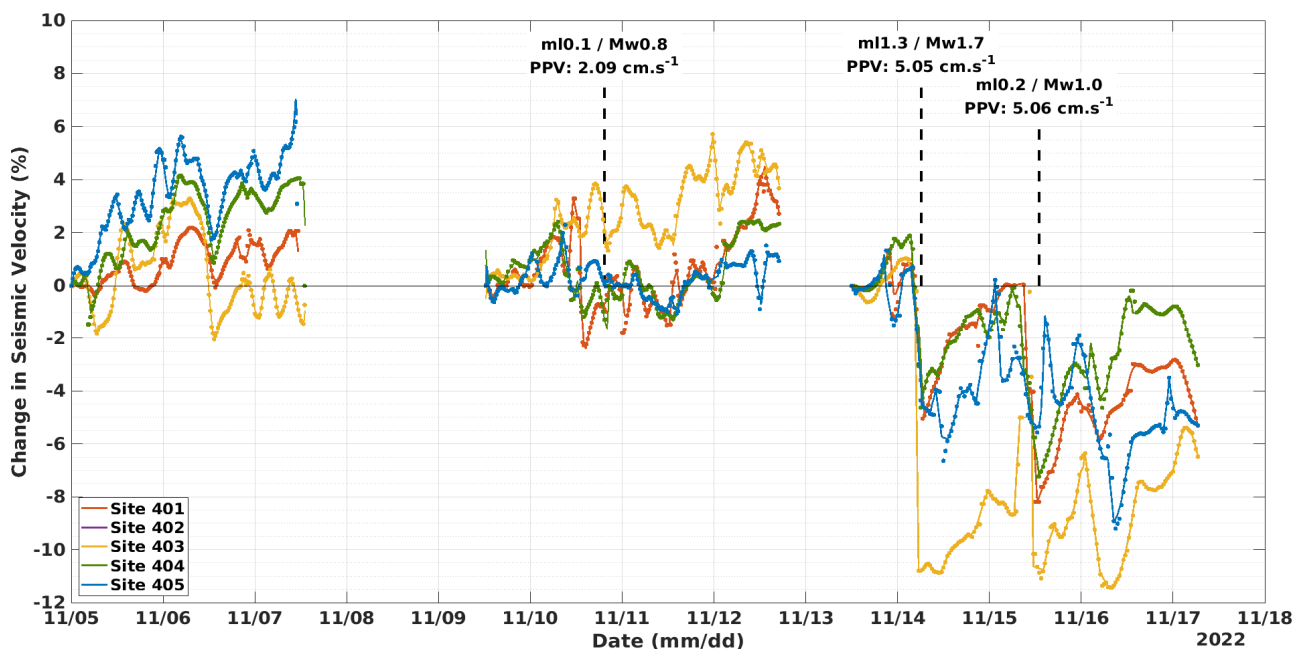
**Figure 11** The piezoelectric source signal velocity variation history

Large events in proximity to the project site are demarcated with dashed vertical black lines in Figure 11. Event magnitude and highest peak ground motion are also quoted on the graph. A clear seismic velocity response was observed for a local magnitude (ML) 1.3 event (moment magnitude 1.7), recorded on the 14 November 2022. Strong ground motions were followed by a clear drop in seismic velocity (maximum of 10.8% drop in velocity) and a post-seismic relaxation response. A development blast also took place on the face adjacent to the project pillar 10 min before the seismic event, making it difficult to attribute this response to blasting alone. The analysis suggests that full recovery (relaxation) did not occur after the event, but this may have been due to the limited duration of monitoring.

5.2.2 Pneumatic source

Velocity change analysis was also performed using the pneumatic source signal; however, due to initial difficulties during the first three months of the project, the source did not produce reliable output.

Continuous and reliable data was recorded between April 2023 and July 2023, and it is important to note that the pillar was fully formed during this period. Results showed direct evidence that the crush pillar was

responding dynamically to seismic events near the project site. These events also induced large decreases in seismic velocity, followed by a characteristic post-seismic relaxation, indicative of material damage followed by gradual healing (Figure 12).
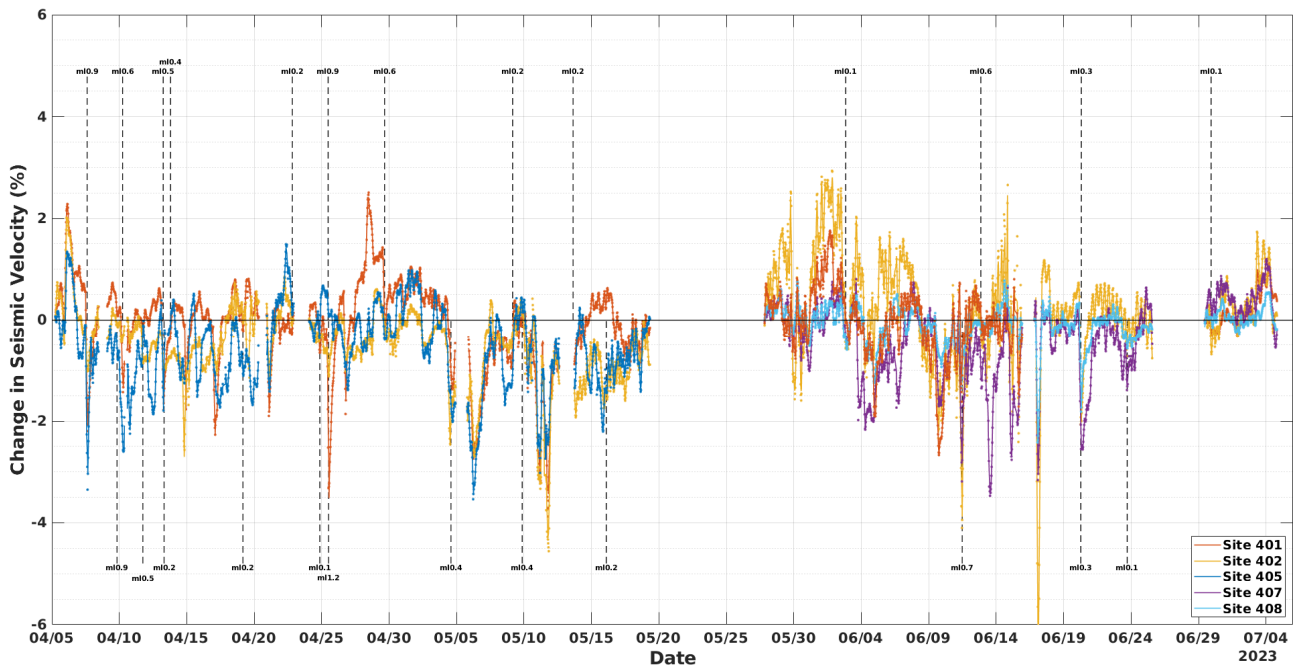
Figure 12   The pneumatic source signal velocity variation history

Multiple instances of this phenomenon were observed during this period, with the largest damage response measured at a 6.2% decrease in seismic velocity. Analysis of seismograms also revealed high peak particle velocities, which suggested that the pillar surface was subjected to strong ground motions during these events. These observations offered valuable insight into the crush pillar behaviour during and after local large events. The velocity variation plot (for 23 hours) is presented in Figure 13. It shows an example of the pillar moving from a minimum velocity change state (steady state) to a maximum velocity state after a seismic event (ML0.9). The negative change in velocity suggests that the rock mass was damaged and fractured. The pillar took a short time (just over five hours) to go back to a 'healing' state and this could be attributed to the crushed fine rock mass that can easily settle back to its 'original' state.
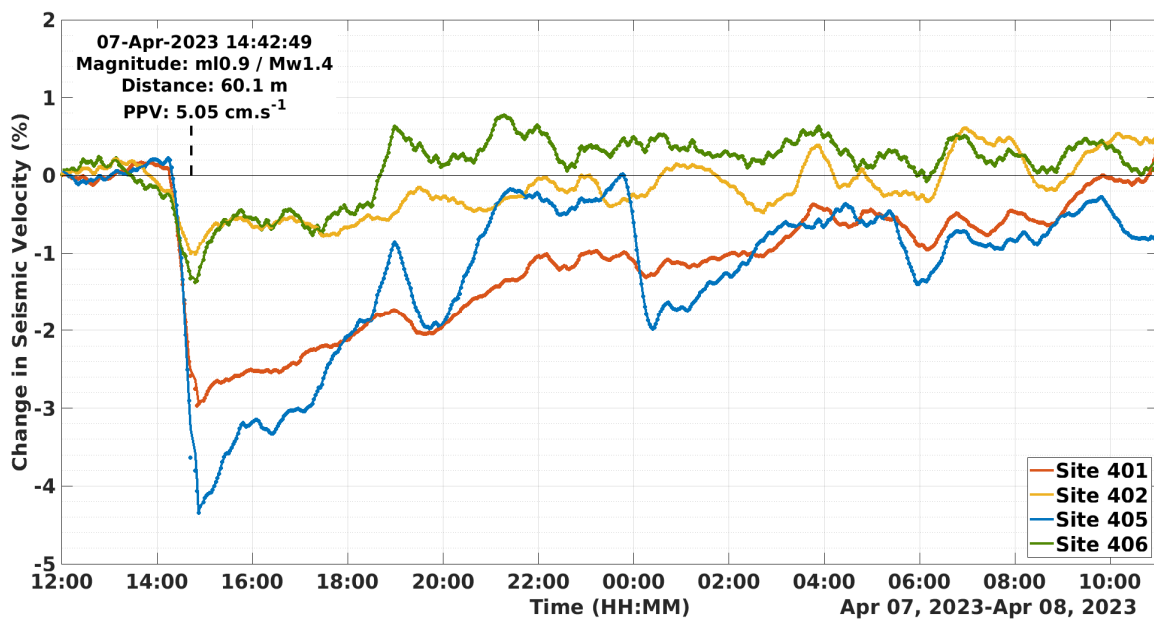
Figure 13   Fracturing and post-relaxation as a result of a ML0.9 event

5.3   Large seismic events response

Analysis of velocity variation histories from both the piezoelectric and pneumatic sources showed a definitive response to the occurrence of large seismic events (ML > 0.0) recorded less than 200 m away from the pillar site. A closer investigation of recorded seismograms revealed that many of these events produced strong ground motions at the pillar surface. Furthermore, the events induced distinctive damage and post-seismic relaxation response in the pillar where the seismic velocity dropped suddenly (indicative of material damage), followed by a gradual increase to the original travel time.

Six cases of large event-induced damage and post-seismic relaxation were considered for closer analysis. Details of the respective events and measured travel time changes are listed in Table 1. Distances were measured from the event hypocentre to the centre of the pillar array and respective peak ground velocity (PGV) are also quoted. Maximum seismic velocity change was measured from the sensor that exhibited the largest drop at the time of the event.

Table 1   details of events, recorded by the mine seismic system, that were selected for post-seismic relaxation analysis

Event no.	Date	Local magnitude (ML)	Moment magnitude (MW)	Distance (m)	PGV (cm/s)	Maximum velocity change (%)
1	2022/11/14	1.3	1.7	70	5.05	12.9
2	2023/04/07	0.9	1.4	61	5.05	4.3
3	2023/04/13	0.5	1.2	70	3.96	2.7
4	2023/04/25	1.2	1.6	89	5.05	3.4
5	2023/06/11	0.7	1.2	78	5.05	2.5
6	2023/06/20	0.3	1.1	107	3.32	4.2

Figure 14 shows a velocity variation plot after a seismic event of ML0.7 and the largest total change was measured at Site 402 (ray path is on the periphery of the pillar, Figure 8), with a drop of 2.5%. Site 408 (ray path is along the core of the pillar, Figure 8) showed the smallest change, which suggests that the core of the pillar was less affected by the ground motion. A ML0.6 seismic event was also recorded the following day; however, it generated significantly lower ground motions at the pillar surface and no clear post-seismic relaxation response was observed in the seismic velocity log.
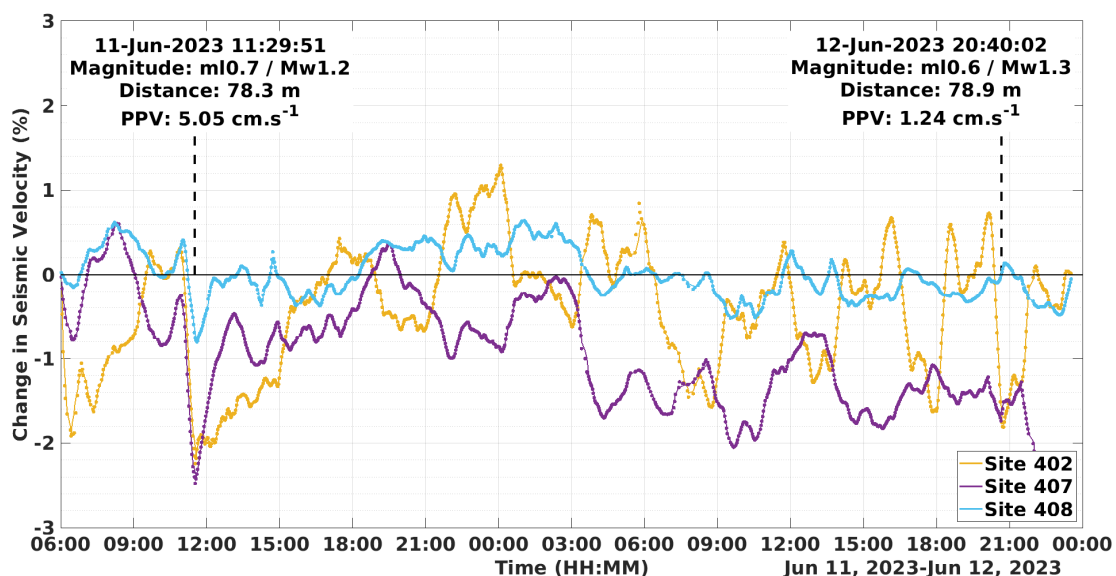
Figure 14   Fracturing and post-relaxation as a result of a ML0.7 event

6   Conclusion

Seismic velocity analysis was performed on data from both the piezoelectric and pneumatic sources. The two sources were never fully operational at the same time; therefore, no direct comparison of the devices was possible. A comparative analysis of the absolute velocity data showed a general increase in seismic velocity (between 5 to 30%), suggesting that the pillar experienced either stiffening or healing over that time.

Piezoelectric source data analysis was performed and from the results the pillar exhibited a distinct response, with immediate material damage (maximum of 10.8% drop in velocity), followed by a gradual period of material healing. Results showed direct evidence that the crush pillar was responding dynamically to significant events, even though the pillar was already fully formed. Some events also induced relatively large decreases in seismic velocity, followed by a characteristic post-seismic relaxation, indicative of material damage followed by gradual healing. Velocity change analysis was also performed using the pneumatic source signal and the results showed direct evidence that the crush pillar was responding dynamically to large events, even though the pillar was already fully formed. Analysis of seismograms also revealed very high peak particle velocities, which suggested that the pillar surface was subjected to strong ground motions during these events, that resulted in a maximum damage response measured as a 6.2% drop in velocity. The results also showed that the increase in velocity never exceeded the original crushing response, therefore, no increase in seismic risk occurred.

The post-seismic relation response was an important observation that provided direct evidence that the crush pillars were responding dynamically to large seismic events. Signal ray paths that passed close to the surface of the pillar had a lower velocity than those that passed through the centre of the pillar. Importantly, the crush pillars behaved well during the seismic events. There is evidence that healing takes place after these events, meaning that the pillars were not permanently weakened by the seismic events.

Acknowledgement

References

Bartels, RH, Beatty, JBC & Barsky, BA 1987, 'An introduction to splines for use in computer graphics and geometric modeling', Morgan Kaufmann Publishers, San Francisco.

Brenguier, F, Campillo, M, Hadziioannou, C & Shapiro, N 2008, 'Postseismic relaxation along the San Andreas Fault at Parkfield from continuous seismological observations', *Science*, vol. 321, No. 5895, pp. 1478–1481.

Chelminski, S, Watson, LM, & Ronen, S 2019, 'Low frequency pneumatic seismic sources', *Geophysical Prospecting*, vol. 67, no. 6, pp. 1547–1556, https://doi.org/10.1111/1365-2478.12774.

Green, M 2023, 'Active seismic source pillar monitoring', *Institute of Mine Seismology 2023 Seminar*, pp. 15–18.

Lynch, RA 2010, 'Passive and active seismic monitoring in mines', keynote address at Deep and High Stress Mining Seminar 2010, Santiago, Chile.

Lynch, RA 2012, 'Active seismic monitoring', in Y Potvin (ed.), *Deep Mining 2012: Proceedings of the Sixth International Seminar on Deep and High Stress Mining*, Australian Centre for Geomechanics, Perth, pp. 201–210, https://doi.org/10.36487/ACG_rep/1201_14_lynch

Mikesell, TD, Malcolm, AE, Yang, D & Haney, MM 2015, 'A comparison of methods to estimate seismic phase delays: numerical examples for coda wave interferometry', *Geophysics Journal International*, vol. 202, No. 1, pp. 347–360.

Niu, F, Silver, PG, Daley, TM, Cheng, X & Majer, EL 2008, 'Preseismic velocity changes observed from active source monitoring at the Parkfields SAFOD drill site', *Nature*, vol. 454, pp. 204–208.

Silver, P, Daley, TM, Niu, F & Majer, EL 2007, 'Active source monitoring of crosswell seismic travel time for stress-induced changes', *Bulletin of the Seismological Society of America*, vol. 97, no. 1B, pp. 281–293.

Watson, BP, Kuijpers, JS, & Stacey, TR 2010, 'Design of Merensky Reef crush pillars', *Journal of the Southern African Institute of Mining and Metallurgy*, vol. 110, no. 10. pp. 581–591.

Watson, BP, Pretorius, W, Mpunzi, P, du Plooy, M, Matthysen, K & Kuijpers, JS 2014, 'Design and positive financial impact of crush pillars on mechanised deep-level mining at South Deep Gold Mine', *Journal of the Southern African Institute of Mining and Metallurgy*, vol. 114, no. 10. pp. 863–880.